Lithium and Vacancy Ordering in T#2−Li_xCoO_2 Derived from O2-Type $LiCoO_2$

Y. Shao-Horn,* F. Weill, L. Croguennec, D. Carlier, M. Ménétrier, and C. Delmas

Institut de Chimie de la Matière Condensée de Bordeaux-CNRS and Ecole Nationale Supérieure de Chimie et Physique de Bordeaux, Université Bordeaux I, 87 av. Dr A. Schweitzer, 33608 Pessac Cedex, France

Received December 30, 2002. Revised Manuscript Received May 14, 2003

Electron diffraction revealed evidence of commensurate and incommensurate superstructures in an unusual phase, T#2, derived from O2-type layered $LiCoO_2$ upon lithium deintercalation. $2a_{orth.} \times 2b_{orth.} \times 2c_{orth.}$, $2a_{orth.} \times b_{orth.} \times c_{orth.}$, and incommensurate with $q = \gamma a^*_{orth.}$ ($\gamma = 0.23$ and 0.36) superstructures were found. It is believed that lithium and vacancy ordering is the most probable cause for the presence of these superstructures. Lithium ordering configurations were discussed in detail with respect to the superstructures observed. It is believed that the presence of various lithium and vacancy ordering configurations improves the stability of the T#2 structure over a range of lithium compositions. Nevertheless, it should be mentioned that the nature of superstructures present and possible lithium ordering configurations in T#2−Li_xCoO_2 were complex and further investigations are needed. In addition, it is of significance to point out that a combination of transmission electron microscopy and electron diffraction showed that three T#2 variants could coexist in different regions within one T#2 crystal, which led to the development of a domain (mazed) microstructure.

Introduction

There are two polymorphic forms of $LiCoO_2$, O3-type, with AB CA BC oxygen packing and O2-type with AB CB AB oxygen packing. O2−$LiCoO_2$, first discovered by Delmas et al.,[1] is metastable to O3−$LiCoO_2$, which is widely used in the positive electrodes of lithium rechargeable batteries. Recently, $LiMO_2$ (M = Ni, Mn, Co, etc.) compounds crystallized in the O2-type crystal structure were reinvestigated for lithium rechargeable battery applications[2−11] as the structural derivatives of O2−$LiMnO_2$ upon lithium deintercalation are stable with respect to the spinel-related framework during electrochemical cycling. In the O2 structure, CoO_6 octahedra share edges with LiO_6 in the layer above and share faces with LiO_6 octahedra in the layer below, as shown in Figure 1. The structure is described in a hexagonal unit cell, $a_{hex.} = 2.8036$ Å and $c_{hex.} = 9.5372$ Å, having space group $P6_3mc$.[4] Lithium removal from O2−$LiCoO_2$ leads to the formation of various novel phases as shown by X-ray powder diffraction (Figure 1), T#2, T#2, and O6, which are closely related to the O2 crystal structure.[4,8,12,13] In addition, differential capacity versus voltage curves reveal the presence of small peaks (just above the background) in the T#2 region, as shown in Figure 1b. It is believed that these peaks could be attributed to ordering transitions in the T#2 region, though the presence of a minute amount of O3−$LiCoO_2$ cannot be excluded completely, which could give rise to some peak intensities in the voltage window where these ordering transitions occur. Although the structural and physical properties of these phases have been well-characterized by in situ and ex situ X-ray and neutron powder diffraction, electrical conductivity, magnetic measurements, and nuclear magnetic resonance studies, the phase stability of T#2 and the interactions between lithium and the vacancy are not clearly understood.

In this study, it is of particular interest to understand the structural stability of T#2 and to investigate lithium and vacancy arrangements in the T#2−Li_xCoO_2 ($0.52 < x \leq 0.72$) phase, in which Co ions reside in octahedral sites and lithium ions partially occupy tetrahedral sites (Figure 1).[4,8,13] The T#2 structure can be related to the O2−Li_xCoO_2 by considering every other CoO_2 slab

* To whom correspondence should be addressed. Present address: Department of Mechanical Engineering, 3-342A, Massachusetts Institute of Technology, 77 Massachusetts Ave., Cambridge, MA 02139. E-mail: shaohorn@mit.edu.

(1) Delmas, C.; Braconnier, J. J.; Hagenmuller, P. *Mater. Res. Bull.* **1982**, *17*, 117.
(2) Siegel, R.; Hirschinger, J.; Carlier, D.; Matar, S.; Ménétrier, M.; Delmas, C. *J Phys. Chem. B* **2001**, *105*, 4166.
(3) Carlier, D.; Saadoune, I.; Suard, E.; Croguennec, L.; Ménétrier, M.; Delmas, C. *Solid State Ionics* **2001**, *144*, 263.
(4) Carlier, D.; Saadoune, I.; Ménétrier, M.; Delmas, C. *J. Electrochem. Soc.* **2002**, *149*, A1310.
(5) Paulsen, J. M.; Thomas, C. L.; Dahn, J. R. *J. Electrochem. Soc.* **2000**, *147*, 861.
(6) Paulsen, J. M.; Dahn, J. R. *J. Electrochem. Soc.* **2000**, *147*, 2478.
(7) Paulsen, J. M.; Thomas, C. L.; Dahn, J. R. *J. Electrochem. Soc.* **2000**, *147*, 2862.
(8) Paulsen, J. M.; Mueller-Neuhaus, J. R.; Dahn, J. R. *J. Electrochem. Soc.* **2000**, *147*, 508.
(9) Paulsen, J. M.; Donaberger, R. A.; Dahn, J. R. *Chem. Mater.* **2000**, *12*, 2257.
(10) Lu, Z.; Dahn, J. R. *J. Electrochem. Soc.* **2001**, *148*, A710.
(11) Lu, Z.; Dahn, J. R. *J. Electrochem. Soc.* **2001**, *148*, A237.
(12) Mendiboure, A.; Delmas, C.; Hagenmuller, P. *Mater. Res. Bull.* **1984**, *19*, 1383.
(13) Carlier, D.; Croguennec, L.; Ceder, G.; Ménétrier, M.; Shao-Horn, Y.; Delmas, C. *Inorg. Chem.*, submitted for publication.

10.1021/cm021816x CCC: $25.00
Published on Web 06/13/2003

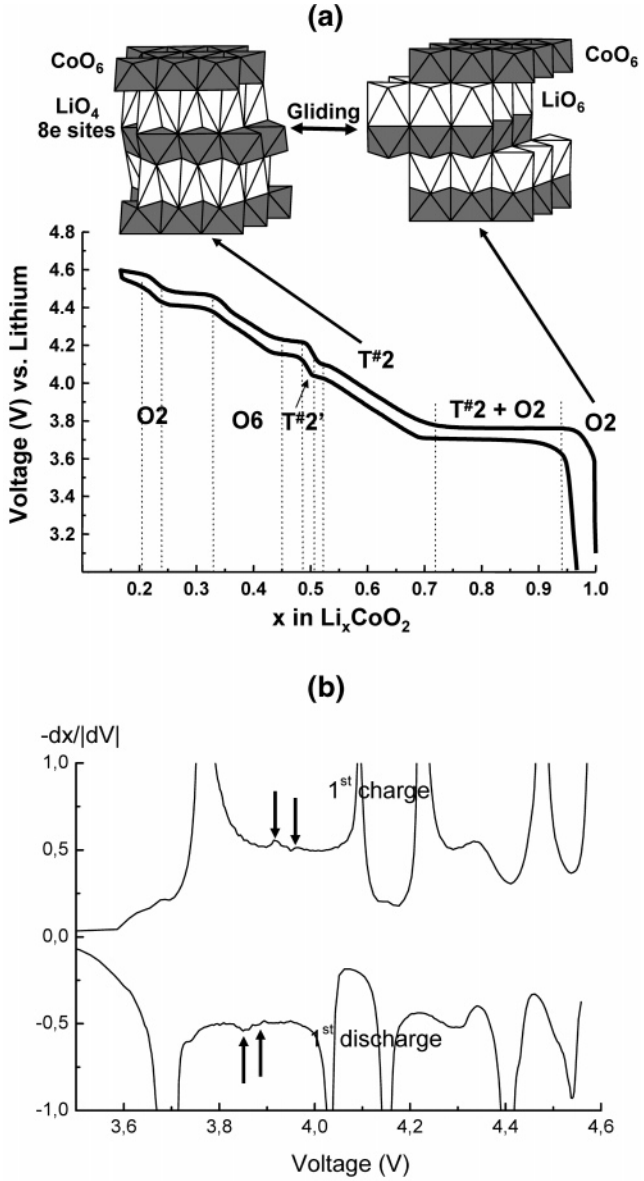

Figure 1. (a) Typical galvanostatic charge and discharge voltage profiles of Li/O2−$LiCoO_2$ cells and schematics of the O2−$LiCoO_2$ structure with both lithium and cobalt ions on the octahedral sites and the T#2−Li_xCoO_2 structure with cobalt ions on the octahedral sites and lithium on the 8e tetrahedral sites. (b) Differential capacity versus voltage plots of first discharge and charge processes of Li/O2−$LiCoO_2$ cells, which shows some minute peaks (marked by arrows) in the T#2 regions.

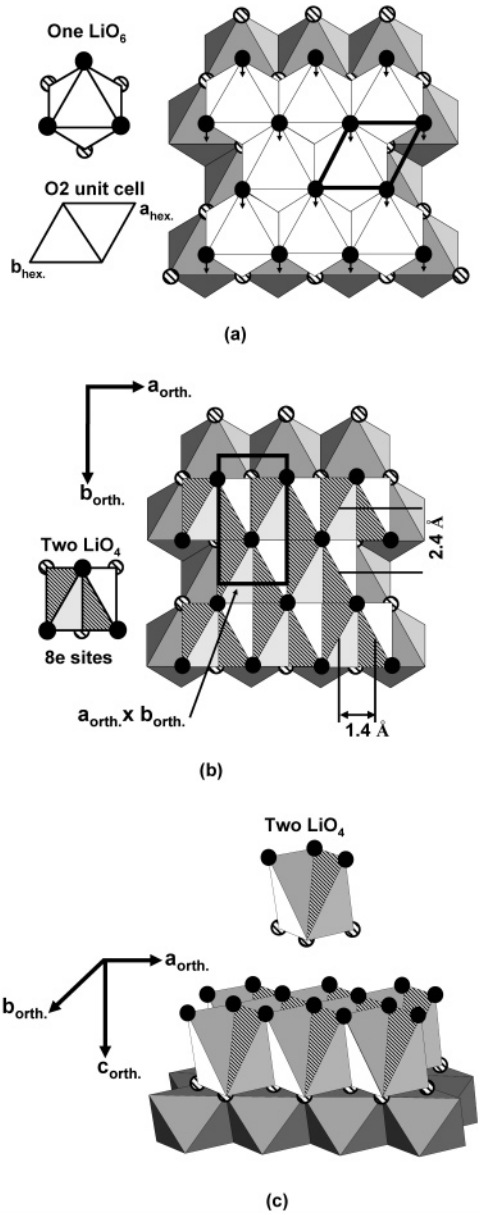

Figure 2. (a) Lithium coordination in LiO_6 octahedra in the O2 structure viewed perpendicular to the CoO_2 slabs, in which the hexagonal cell is outlined in solid; the arrows indicate the displacement of the oxygen atoms of the top layer of the edge-sharing LiO_6 octahedra associated with the O2−T#2 transition; (b) lithium coordination in the 8e LiO_4 tetrahedra in the T#2−Li_xCoO_2 structure viewed perpendicular to the CoO_2 slabs, with the orhombic cell outlined; (c) the 8e LiO_4 tetrahedra in (b) viewed along the $b_{orth.}$ direction.

gliding in three possible directions such as ($^1/_3$, $^1/_6$, 0), as shown in Figure 2a. This gliding leads to an usual oxygen packing with the oxygen atoms no longer on the A, B, and C positions of a regular triangular lattice, which reduces the crystal symmetry to orthorhombic (the unit cell outlined in Figure 2b). For example, "T#2−$Li_{0.61}CoO_2$" has an orthorhombic unit cell, with $a_{orth.}$ = 2.8097 Å, $b_{orth.}$ = 4.8500 Å, $c_{orth.}$ = 9.9082 Å, and space group *Cmca*.[4] Previous studies[9,13] have reported that lithium ions are located on the 8e-type tetrahedral sites in the T#2 structure, as shown in Figure 2b (projected along the $c_{orth.}$ axis) and Figure 2c (projected along the $b_{orth.}$ axis). It should be noted that there are two 8e sites available per cobalt ion and fewer than half of the 8e sites are occupied by lithium ions in the T#2−Li_xCoO_2 structure. As simultaneous occupancy of adjacent 8e sites is unlikely due to small site-to-site distances (1.4 and 2.4 Å), lithium ordering on the 8e sites is expected in the T#2 structure. First-principles calculations have predicted that lithium ordering on the 8e sites in the T#2 structure is thermodynamically stable and $3a_{orth.} \times b_{orth.} \times c_{orth.}$ and $2a_{orth.} \times b_{orth.} \times c_{orth.}$ superstructures are expected at the $Li_{2/3}CoO_2$ and $Li_{0.5}CoO_2$ compositions, respectively.[13] However, no evidence of lithium and vacancy ordering was revealed by the recent neutron powder diffraction study as there were no additional reflections found to those of the T#2 phase.[13] This result is not surprising as neutron powder diffraction simulation shows that the superreflection intensi-

ties associated with lithium and vacancy ordering are too weak (on the order of the background noise) to be resolved experimentally.[14]

Understanding lithium and vacancy ordering in the T#2 structure would provide essential insights into the formation and structural stability of this novel T#2−Li_xCoO_2 phase. Electron diffraction is more sensitive to lithium in comparison to X-ray and neutron diffraction and recent single-crystal electron diffraction analyses have clearly revealed super-reflections associated with lithium ordering in O3-type $Li_{0.5}CoO_2$ and Li_xNiO_2 phases.[15−17] Therefore, in this study, we undertake an electron diffraction study to probe lithium and vacancy ordering in two single-phase T#2−Li_xCoO_2 ($x = 0.7$ and $x = 0.63$) samples.

It is also of interest to study the mechanism by which the T#2 phase is nucleated and grown from O2−$LiCoO_2$ upon lithium removal on the nanometer scale. As reported from previous X-ray powder diffraction analyses,[4,8] the O2−T#2 transformation is accompanied by a dramatic change in the *c* lattice parameter (nearly 4%). It is believed that the T#2 formation in the platelike O2 crystals would cause considerable strains and stresses on the microscopic scale.[3] Therefore, the microstructural development during this phase transformation would be driven by minimization of the overall strains and stresses within each individual crystal. In this study, we combine electron diffraction and transmission electron microscope imaging analyses to study two slightly deintercalated O2−Li_xCoO_2 samples in an attempt to provide new insights into the mechanism by which the O2−T#2 phase transformation occurs.

Experimental Section

An O2−"$LiCoO_2$" sample was synthesized by an ion-exchange process from $Na_{0.7}CoO_2$ as detailed in ref 3. An "$Li_{0.63}CoO_2$" compound was prepared electrochemically through lithium deintercalation from the O2−$LiCoO_2$ sample in an Li/1M$LiClO_4$−PC/Li_xCoO_2 cell under galvanostatic conditions with a current density of C/100, in which 1 C current density corresponds to extraction of one electron per $LiCoO_2$ within 1 h. The $LiCoO_2$ electrode consisted of 88% of $LiCoO_2$, 2% of polytetrafluorethylene, and 10% of carbon (graphite and carbon black in 1:1) in weight. An "$Li_{0.7}CoO_2$" sample was obtained from a chemical deintercalation in a 10 M bromine solution dissolved in anhydrous acetonitrile as reported previously.[13] To understand the O2−T#2 transformation, two slightly deintercalated samples, "$Li_{0.95}CoO_2$" and "$Li_{0.94}CoO_2$" were also prepared from electrochemical deintercalation. The phase purity of these "Li_xCoO_2" samples was examined by X-ray powder diffraction with Cu Kα on a Siemens D5000 diffractometer. The structural parameters of $Li_{0.63}CoO_2$ and $Li_{0.7}CoO_2$ samples were determined from Rietveld refinements of their experimental X-ray powder diffraction patterns,[18] which were collected between 10° and 120° of 2θ with a step size of 0.02° and a step time of 40 s at room temperature. Single-crystal electron diffraction patterns and transmission electron microscope images were also collected from these powder samples suspended on a copper grid with lacey carbon under an accelerating voltage of 200 keV on a JEOL 2000FX microscope.

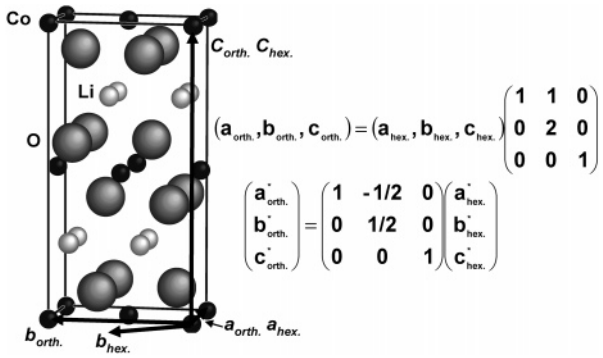

Figure 3. Crystallographic relationship between the O2−$LiCoO_2$ structure and the T#2−Li_xCoO_2 structure in the real and reciprocal space.

Results and Discussion

X-ray Powder Diffraction Analysis. X-ray powder diffraction analyses showed that the O2−$LiCoO_2$, $Li_{0.7}CoO_2$, and $Li_{0.63}CoO_2$ samples were nearly phase pure. Structural refinements showed that the structural parameters of these samples were consistent with those of the O2 and T#2 structures reported previously.[4] Both the $Li_{0.95}CoO_2$ and $Li_{0.94}CoO_2$ samples were found to predominantly consist of the O2 phase with a small amount of T#2, which was expected as they were near the composition limit where the O2−T#2 phase transformation began.[4,8]

Electron Diffraction Evidence of Lithium Ordering in T#2. Electron diffraction patterns collected from the chemically delithiated $Li_{0.7}CoO_2$ and electrochemically deintercalated $Li_{0.95}CoO_2$, $Li_{0.94}CoO_2$, and $Li_{0.63}CoO_2$ samples were indexed according to the O2 or the T#2 structure. The crystallographic relationships between these two structures in the real and reciprocal space are shown in Figure 3. In addition to fundamental reflections of the T#2 structure, additional reflections were revealed in the electron diffraction patterns collected from these samples. As cobalt and oxygen atoms fully occupy the 4a and 8f sites in the T#2 structure, respectively, there is no possible ordering of cobalt and oxygen allowed in the structure, which is consistent with previous experimental X-ray and neutron powder diffraction results.[4,13] Therefore, it is believed that the presence of these additional reflections is attributed to lithium and vacancy ordering in the T#2 structure. Lithium and vacancy ordering configurations in a $2a_{orth.} \times 2b_{orth.} \times 2c_{orth.}$ and $2a_{orth.} \times b_{orth.} \times c_{orth.}$ commensurate superstructures and an incommensurate superstructure with $q = \gamma a^*_{orth.}$ ($\gamma = 0.23-0.36$) of the parent T#2 phase were proposed and used to explain the super-reflections observed in the experimental electron diffraction patterns, as detailed in the following discussions.

$2a_{orth.} \times 2b_{orth.} \times 2c_{orth.}$ Commensurate Superstructure. Electron diffraction patterns collected from two regions in one T#2−$Li_{0.7}CoO_2$ crystal along the $[10\bar{1}]_{orth.}$ zone axis are shown in Figure 4a,b. Only the fundamental reflections of the T#2 structure are present in Figure 4a. In contrast, in addition to the fundamental reflections, additional weak super-reflections halfway between the center of diffraction and the fundamental reflections were observed in Figure 4b. The presence of these super-reflections indicates doubling of the unit cell dimensions of the T#2 structure, which corresponds to

(14) Carlier, D. Ph.D. Dissertation, Université Bordeaux I, 2001.
(15) Pérès, J. P.; Weill, F.; Delmas, C. *Solid State Ionics* **1999**, *116*, 19.
(16) Delmas, C.; Ménétrier, M.; Croguennec, L.; Levasseur, S.; Pérès, J. P.; Pouillerie, C.; Prado, G.; Fournès, L.; Weill, F. *Int. J. Inorg. Mater.* **1999**, *1*, 11.
(17) Shao-Horn, Y.; Levasseur, S.; Weill, F.; Delmas, C. *J. Electrochem. Soc.* **2003**, *150*, A366−A373.
(18) Rodriguez-Carjajal, J. *J. Physica B* **1993**, *192*, 55.

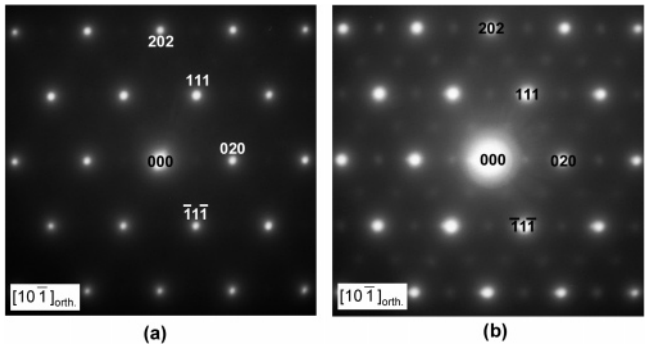

Figure 4. Electron diffraction patterns collected from two regions in one T#2−$Li_{0.7}CoO_2$ crystal along the $[10\bar{1}]_{orth.}$ zone axis (a) having only the fundamental reflections indexed consistently to the T#2 structure and (b) showing the fundamental reflections and super-reflections corresponding to a $2a_{orth.} \times 2b_{orth.} \times 2c_{orth.}$ superstructure.

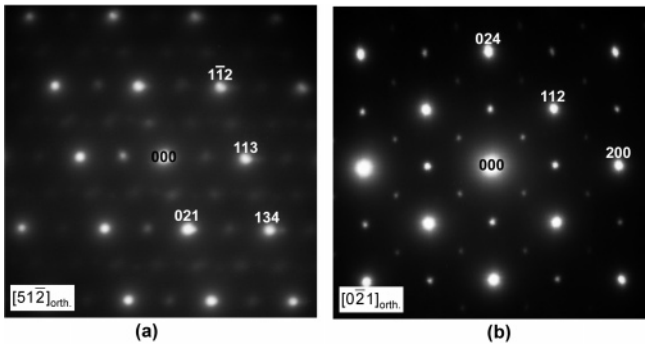

Figure 5. (a) The $[51\bar{2}]_{orth.}$ and (b) the $[02\bar{1}]_{orth.}$ diffraction patterns collected from the $Li_{0.7}CoO_2$ sample, which is consistent with the presence of the $2a_{orth.} \times 2b_{orth.} \times 2c_{orth.}$ superstructure.

a $2a_{orth.} \times 2b_{orth.} \times 2c_{orth.}$ superstructure. This superstructure was found in many other electron diffraction patterns collected from the $Li_{0.7}CoO_2$ sample; the $[51\bar{2}]_{orth.}$ and the $[02\bar{1}]_{orth.}$ diffraction patterns are shown for examples in parts (a) and (b), respectively, of Figure 5, in which the strong reflections are indexed consistently to the T#2 structure. The systematic extinctions exhibited in these patterns suggest the existence of a "C" Bravais lattice. As super-reflections of this superstructure were also observed (though to a smaller extent) in the electron diffraction patterns collected from the other three samples studied, it is believed that it is present in a large composition range of the T#2−Li_xCoO_2 structure.

The $2a_{orth.} \times 2b_{orth.} \times 2c_{orth.}$ superstructure evidenced by electron diffraction can be related to the ordering of lithium and vacancy on the 8e sites of the parent T#2 structure. To describe the doubling of the $a_{orth.}$ and $b_{orth.}$ cell parameters, a possible lithium and vacancy ordering configuration is proposed in Figure 6: two variants, Variant I and II, are allowed as two orientations exist for the 8e LiO_4 tetrahedra in the T#2 structure. As shown, the lithium and vacancy ordering configuration corresponds to two different LiO_4 tetrahedra rows alternatively placed along the $b_{orth.}$ axis: one having lithium ions ordered on every other 8e sites and the other with lithium ions ordered on every fourth 8e sites. It should be noted that all these tetrahedra occupied by lithium share only corners. The doubling of the $c_{orth.}$ cell parameter results from alternation of these variants

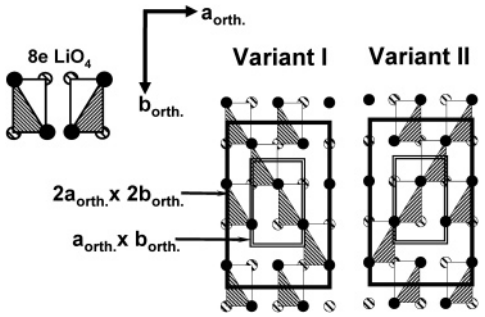

Figure 6. Lithium and vacancy ordering proposed to describe the doubling of the $a_{orth.}$ and $b_{orth.}$ cell parameters. Note that two variants are allowed as two possible orientations exist for the 8e LiO_4 tetrahedra. The doubling of the $c_{orth.}$ cell parameter results from the alternation of these variants in the interslab space along the $c_{orth.}$ axis.

in the interslab spaces along the $c_{orth.}$ axis. These 8e sites can be completely or partially occupied by lithium, which allows the $2a_{orth.} \times 2b_{orth.} \times 2c_{orth.}$ superstructure to accommodate a range of lithium compositions in the T#2 phase. For example, full occupancy of these LiO_4 tetrahedra in the superstructure (Figure 6) corresponds to the $Li_{0.75}CoO_2$ composition. This is consistent with the fact that the T#2−Li_xCoO_2 phase is stable over a large range of lithium compositions (Figure 1).[4] Similar ordering configurations have been reported for the monoclinic Li_xNiO_2 ($0.5 \leq \times \leq 0.75$)[15] and the Na_xCoO_2[19] solid solution phases.

Although other configurations of lithium and vacancy ordering in the $2a_{orth.} \times 2b_{orth.} \times 2c_{orth.}$ supercell might exist, the proposed ordering arrangements are consistent with the extinction conditions exhibited in the experimental electron diffraction patterns collected in this study. It should be mentioned that this $2a_{orth.} \times 2b_{orth.} \times 2c_{orth.}$ superstructure was not considered in the previous first-principles computation study of lithium and vacancy ordering in T#2−Li_xCoO_2.[13]

$2a_{orth.} \times b_{orth.} \times c_{orth.}$ Commensurate Superstructure. In addition to the $2a_{orth.} \times 2b_{orth.} \times 2c_{orth.}$ superstructure, evidence of a $2a_{orth.} \times b_{orth.} \times c_{orth.}$ superstructure was revealed in the $Li_{0.7}CoO_2$ sample. Single-crystal electron diffraction patterns collected from the $Li_{0.7}CoO_2$ sample along the $[0\bar{1}1]_{orth.}$ and $[11\bar{1}]_{orth.}$ zone axes are shown in parts (a) and (b), respectively, of Figure 7, in which the fundamental reflections are indexed consistently to the T#2 structure. The additional weak reflections in these patterns cannot be explained by the T#2 structure but they can be indexed to a $2a_{orth.} \times b_{orth.} \times c_{orth.}$ supercell. The experimental patterns in (a) and (b) of Figure 7 are reindexed according to this supercell in (c) and (d), respectively, of Figure 7. Super-reflections of this superstructure were also observed in some of the electron diffraction patterns collected from the $Li_{0.94}CoO_2$ sample that contained a small amount of the T#2 phase. The presence of such a $2a_{orth.} \times b_{orth.} \times c_{orth.}$ supercell can be related to lithium (shown as LiO_4 tetrahedra) and vacancy ordering on every other 8e site and every fourth 8e site in the parent T#2 structure along the $a_{orth.}$ axis, as shown in Figure 8. Full or partial occupancy of the LiO_4 tetrahedra allows the $2a_{orth.} \times b_{orth.} \times c_{orth.}$ superstructure to accommodate a range of lithium composi-

(19) Fouassier, C.; Matejka, G.; Reau, J. M.; Hagenmuller, P. *J. Solid State Chem.* **1973**, *6*, 532.

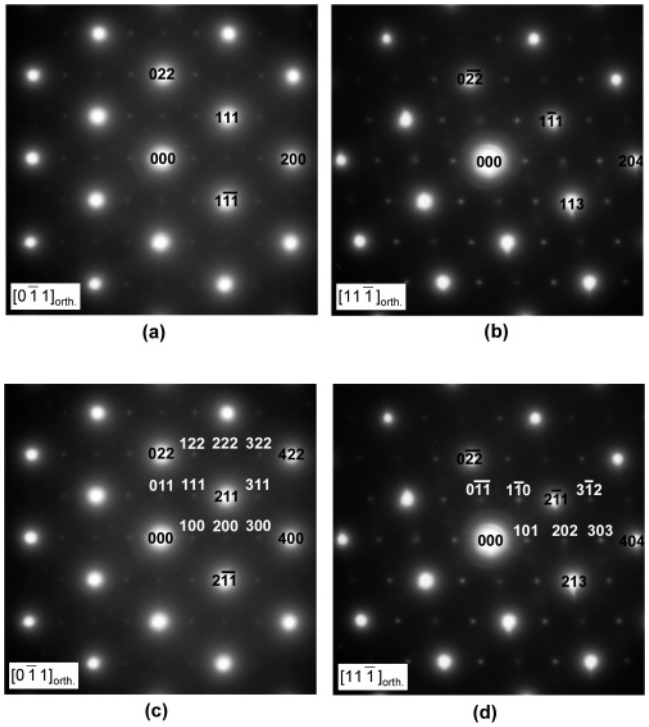

Figure 7. Single-crystal electron diffraction patterns collected from the $Li_{0.7}CoO_2$ sample along the (a) $[0\bar{1}1]_{orth.}$ and (b) $[11\bar{1}]_{orth.}$ zone axes, which reveals super-reflections corresponding to a $2a_{orth.} \times b_{orth.} \times c_{orth.}$ superstructure. The fundamental reflections are indexed to the T#2 structure. The diffraction patterns (a) and (b) are reindexed to the $2a_{orth.} \times b_{orth.} \times c_{orth.}$ supercell in (c) and (d), respectively.

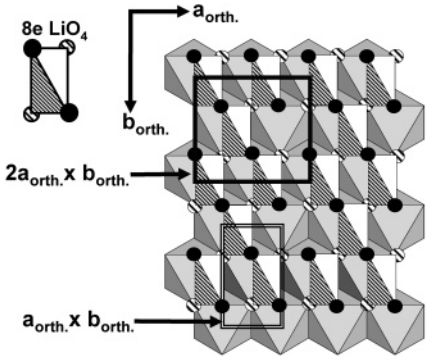

Figure 8. Proposed ordering configuration of lithium and vacancy that could lead to a $2a_{orth.} \times b_{orth.} \times c_{orth.}$ superstructure of the parent T#2 structure.

tions in the T#2 structure, similar to the $2a_{orth.} \times 2b_{orth.} \times 2c_{orth.}$ superstructure discussed earlier. The extinction conditions exhibited in the experimental electron diffraction patterns indicated that this $2a_{orth.} \times b_{orth.} \times c_{orth.}$ superstructure could have a space group symmetry of *Pmmm*. It should be mentioned that this superstructure (Figure 8) present in $Li_{0.7}CoO_2$ and $Li_{0.94}CoO_2$ does not exhibit the same extinction conditions as the $2a_{orth.} \times b_{orth.} \times c_{orth.}$ superstructure of $Li_{0.5}CoO_2$ predicted previously by first-principles calculations.[13] For example, the (100), (101), and (011) reflections are not allowed by the symmetry of the $2a_{orth.} \times b_{orth.} \times c_{orth.}$ superstructure of $Li_{0.5}CoO_2$ but these superreflections are present in Figure 7. This difference in lithium ordering is to be expected as the ordering configurations could be highly dependent on the chemical composition of Li_xCoO_2.

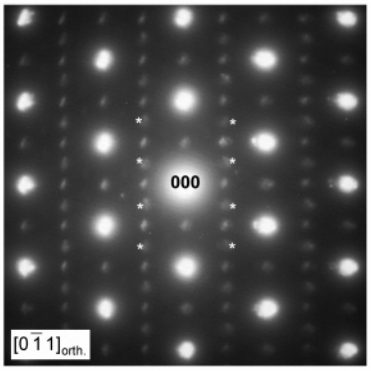

Figure 9. The $[0\bar{1}1]_{orth.}$ electron diffraction pattern collected from $Li_{0.94}CoO_2$, where reflections corresponding to both the $2a_{orth.} \times b_{orth.} \times c_{orth.}$ and $2a_{orth.} \times 2b_{orth.} \times 2c_{orth.}$ superstructures were revealed. The reflections unique to the $2a_{orth.} \times 2b_{orth.} \times 2c_{orth.}$ superstructure are marked by *.

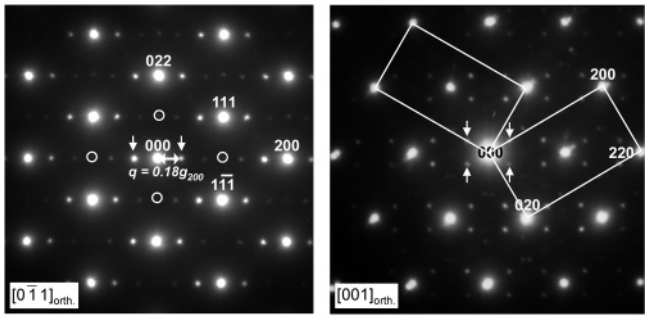

Figure 10. (a) The $[0\bar{1}1]_{orth.}$ and (b) $[001]_{orth.}$ electron diffraction patterns collected from the $Li_{0.63}CoO_2$ samples, where the first-order, incommensurate reflections are marked by arrows.

It should be noted that the ordering configuration of lithium and vacancy in the $2a_{orth.} \times b_{orth.} \times c_{orth.}$ supercell (Figure 8) is very similar to those of the $2a_{orth.} \times 2b_{orth.} \times 2c_{orth.}$ superstructure perpendicular to the $c_{orth.}$ axis (Figure 6). These two superstructures only differ in the positions of lithium ions and vacancies where lithium ions order every fourth 8e site along the $a_{orth.}$ direction. The $[0\bar{1}1]_{orth.}$ electron diffraction pattern collected from the $Li_{0.94}CoO_2$ sample is shown in Figure 9, which consists of both sets of superreflections characteristic of each superstructure. In comparison to Figure 7a (along the same zone axis as Figure 9), additional reflections marked by * were noted in Figure 9, which could be indexed consistently to the $2a_{orth.} \times 2b_{orth.} \times 2c_{orth.}$ superstructure. The distortion of the super-reflection points in Figure 9 was noted but the cause for this distortion was not understood. Therefore, the $2a_{orth.} \times b_{orth.} \times c_{orth.}$ and $2a_{orth.} \times 2b_{orth.} \times 2c_{orth.}$ superstructures were found to coexist within one T#2−Li_xCoO_2 crystal. It is believed that the Gibbs free energy difference of these two superstructures could be negligible.

Incommensurate Structure $q = \gamma a^*_{orth.}$ ($\gamma = 0.23-0.36$). In addition to the commensurate superstructures discussed above, incommensurate periodicity was observed along the $a_{orth.}$ axis of the T#2−Li_xCoO_2 structure. The $[0\bar{1}1]_{orth.}$ and $[001]_{orth.}$ electron diffraction patterns collected from the $Li_{0.63}CoO_2$ sample are shown in parts (a) and (b), respectively, of Figure 10, where the first-order, incommensurate reflections are marked by arrows. It should be noted that the super-reflections

expected from the $2a_{orth.} \times 2b_{orth.} \times 2c_{orth.}$ and $2a_{orth.} \times b_{orth.} \times c_{orth.}$ superstructures are not present in these patterns. As indicated in Figure 10a, the incommensurate periodicity q was found to be equal to $0.18 \cdot \mathbf{g}_{200}$ of the T#2 structure, which is equivalent to $0.36 \cdot a^*_{orth.}$. The origin of these extra reflections present between the second-order incommensurate satellites of two fundamental reflections along the $a^*_{orth.}$ direction (marked by circles in Figure 10a) is not understood. Two orientation states of the identical incommensurate periodicity, $q = 0.36 \cdot a^*_{orth.}$, were observed in Figure 10b, and two rectangular frames were drawn to show the relative rotation of the two T#2 variants. In addition, an incommensurate periodicity of $q = 0.23 \cdot a^*_{orth.}$ was found in other crystals of the $Li_{0.63}CoO_2$ sample. Therefore, it is believed that the incommensurate periodicity could vary from crystal to crystal. The incommensurate or nonintegral periodicity can be related to incommensurate ordering of lithium and vacancy in the T#2−Li_xCoO_2 structure, which can result from the mixing of domains having distinct a-dimension of the T#2 parent structure. It should be noted that the experimentally observed values of the incommensurate vector q, $0.36 \cdot a^*_{orth.}$ and $0.23 \cdot a^*_{orth.}$, are near commensurate superstructures of $^1/_3 \cdot a^*_{orth.}$ ($q = 0.33$) and $^1/_4 \cdot a^*_{orth.}$ ($q = 0.25$), respectively. Vast examples of incommensurate structures induced by modulation in the chemical composition on the atomic scale exist in the literature.[20] For example, an incommensurate structure with modulation spacing of 2.2 times c (each subcell contains two alkali sites in the c direction of the subcell) has been observed in A_xWO_3 phases (A: alkali element) while every fourth or fifth alkali site is unoccupied.[20] Therefore, we believe that incommensurate structures observed in the T#2 region can be explained by variation of lithium and vacancy ordering configurations along the a-axis of T#2 parent structure.

Microstructural Characterization of T#2. Electron diffraction and transmission electron microscope imaging analyses were combined to study the microstructure of the T#2 phase in the slightly deintercalated $Li_{0.95}CoO_2$ and $Li_{0.94}CoO_2$ samples to provide new insights into the mechanism of the O2−T#2 phase transformation. As expected from the chemical compositions and X-ray powder diffraction results, most of the electron diffraction patterns collected from these two samples can be indexed consistently to the O2 structure and do not contain any additional super-reflections. Some crystals were shown to have the $2a_{orth.} \times 2b_{orth.} \times 2c_{orth.}$ and $2a_{orth.} \times b_{orth.} \times c_{orth.}$ superstructures, which could be related to lithium and vacancy ordering in the T#2 structure as discussed previously.

As mentioned previously, the formation of the T#2 structure from O2−Li_xCoO_2 requires every other CoO_2 slab to glide halfway between two hexagonal lattice points in the basal plane (Figure 2). It is believed that such a gliding is induced by strong electrostatic repulsion between adjacent CoO_2 slabs upon lithium deintercalation. There are three equivalent directions for this gliding in the O2−$LiCoO_2$ structure, and thus three possible orientation states (variants) exist for nucleation of the T#2. Coexistence of these variants in one T#2 crystal would lead to the development of a domain

(20) Buseck, P. R.; Cowley, J. M. *Am. Mineral.* **1983**, *68*, 18.

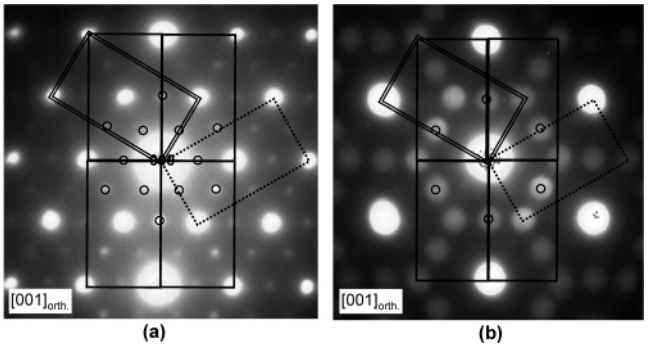

Figure 11. Two types of the $[001]_{orth.}$ single-crystal electron diffraction patterns collected from the $Li_{0.94}CoO_2$ sample, which contain the super-reflections of the (a) $2a_{orth.} \times 2b_{orth.} \times 2c_{orth.}$ and (b) $2a_{orth.} \times b_{orth.} \times c_{orth.}$ superstructures.

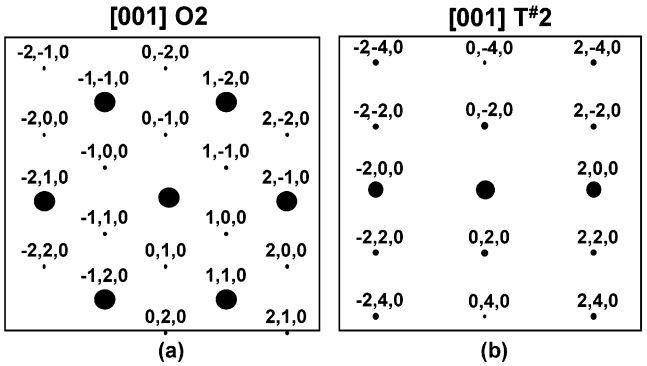

Figure 12. Simulated single-crystal electron diffraction pattern of (a) the O2 structure along the $[001]_{hex.}$ direction and (b) the T#2 structure of the $[001]_{orth.}$ direction.

(mazed) microstructure. In this study, electron diffraction evidence was found for the domain (or mazed) microstructure on the nanometer scale in T#2−Li_xCoO_2 electrochemically derived from O2−$LiCoO_2$, similar to those reported in the O3−$Li_{0.5}CoO_2$[17] and Li_xNiO_2 systems.[15] Two types of the $[001]_{orth.}$ single-crystal electron diffraction patterns collected from the $Li_{0.94}CoO_2$ sample were observed, as shown in parts (a) and (b), respectively, of Figure 11. The simulated electron diffraction patterns of the O2 and T#2 structures are shown for comparison in parts (a) and (b), respectively, of Figure 12. Fundamental reflections of these two structures can be found in these patterns (Figure 11a,b); however, it is evident that these two structures alone cannot account for all of the reflections observed. The additional reflections present can be explained consistently by considering the fact that (1) a domain microstructure exists for the T#2 phase and (2) lithium ions and vacancies order in the $2a_{orth.} \times 2b_{orth.} \times 2c_{orth.}$ (Figure 11a) or $2a_{orth.} \times b_{orth.} \times c_{orth.}$ (Figure 11b) superstructures. Solid, dashed, and doubled lines are drawn in the patterns to show the relative rotation of the three variants of T#2. The superreflections unique to the $2a_{orth.} \times 2b_{orth.} \times 2c_{orth.}$ and $2a_{orth.} \times b_{orth.} \times c_{orth.}$ superstructures are marked by solid circles in parts (a) and (b), respectively, of Figure 11. For example, the marked reflections in Figure 11b can only be indexed to the (100)-type reflections of the $2a_{orth.} \times b_{orth.} \times c_{orth.}$ superstructure. Overlapping of all three variants of the superstructures of T#2 can generate all of the reflections observed in the experimental patterns, which is consistent with the changes in crystal symmetry from O2 to

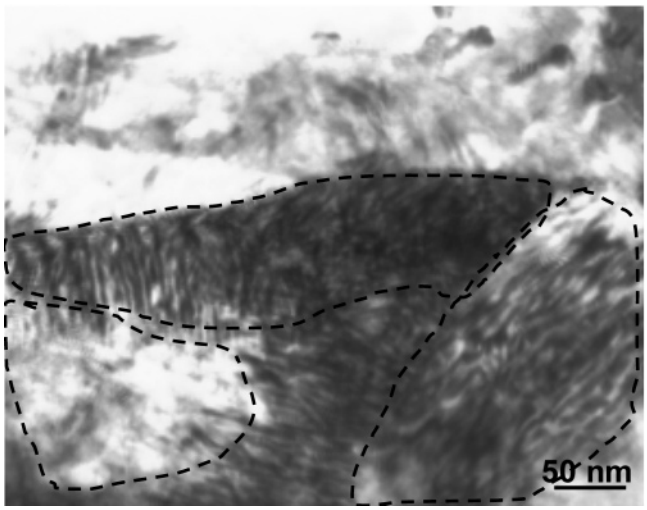

Figure 13. Bright-field transmission electron microscope image of the region where the electron diffraction pattern in Figure 11a was collected, which clearly revealed that the domain size was on the order of 100−200 nm. The domain boundaries are marked by dashed lines.

T#2 shown in Figure 2a. It should be mentioned that none of the $[001]_{orth.}$ zone axis patterns collected from the $Li_{0.95}CoO_2$, $Li_{0.94}CoO_2$, $Li_{0.7}CoO_2$, and $Li_{0.63}CoO_2$ samples resemble the simulated pattern of single-crystal T#2 in Figure 12b. Therefore, it is believed that the domain microstructure might be present in all T#2 crystals.

A bright-field transmission electron microscope image of the region where the electron diffraction pattern in Figure 11b was collected is shown in Figure 13. Assuming the region has uniform thickness perpendicular to the $[001]_{orth.}$ direction (parallel to the electron beam direction), the intensity variation in the image can be attributed to diffraction contrast of different domains in the region. The T#2 variant size was shown on the order of 100−200 nm. In addition, it is believed that the striations in Figure 13, similar to those observed in the monoclinic O3−Li$_x$CoO$_2$ crystals, are attributed to strains present within each domain. It is interesting to note that the domain sizes of T#2 induced by electrostatic repulsion of CoO_2 slabs upon lithium removal from O2−$LiCoO_2$ are considerably greater than those (50 nm) found in the monoclinic O3−Li$_x$CoO$_2$ crystals associated with lithium and vacancy ordering.

General Discussions

In this study, electron diffraction showed the presence of commensurate and incommensurate superstructures in T#2−Li$_x$CoO$_2$ samples. Super-reflections observed in the experimental electron diffraction patterns were correlated with lithium and vacancy ordering on the 8e tetrahedral sites in a $2a_{orth.} \times 2b_{orth.} \times 2c_{orth.}$ or a $2a_{orth.} \times b_{orth.} \times c_{orth.}$ superstructure. These two superstructures can be present in different regions within one T#2 crystal. Partial occupancy of lithium on the 8e sites allows both superstructures to accommodate a range of lithium compositions, which is consistent with the stability of the T#2−Li$_x$CoO$_2$ phase. In addition to lithium ordering in commensurate superstructures, incommensurate periodicity $q = 0.36 \cdot a^*_{orth.}$ or $0.23 \cdot a^*_{orth.}$ in the electron diffraction patterns is related to incommensurate ordering of lithium and vacancy. It is believed that incommensurate ordering is preferred to commensurate ordering of lithium and vacancy in large superstructures such as $3a_{orth.} \times b_{orth.} \times c_{orth.}$ and $4a_{orth.} \times b_{orth.} \times c_{orth.}$. It should be mentioned that, in all of the proposed ordered structures, lithium ions occupy the 8e sites in the T#2 structure. Electron diffraction evidence of commensurate and incommensurate superstructures presented in our manuscript alone cannot exclude the possibilities that (1) lithium ions can occupy tetrahedral sites ($8f_{edges}$ and $8f_{face}$) other than 8e sites nor (2) other lithium and vacancy ordering configurations than the ones described in our manuscript exist in the T#2 structure. Although the commensurate and incommensurate structures might be found stable within different ranges of lithium compositions of the T#2 structure, there is not enough experimental evidence to assign a specific lithium composition window for each of these superstructures observed.

It should be noted that the voltage-capacity profile for the entire T#2 compositional range is relatively smooth and only minute peaks were noted in the different capacity versus voltage curves (Figure 1b), which reflects little evidence of lithium and ordering in the T#2 phase. In this study, it is hypothesized that the lack of substantial peaks of ordering transitions within the single-phase T#2−Li$_x$CoO$_2$ domain in the differential capacity versus voltage curve (Figure 1b) could be attributed to the presence of a large number of commensurate and incommensurate superstructures with similar Gibbs free energies of different chemical compositions. The presence of many ordered phases in the T#2 region is supported by a recent first-principles study,[21] though this theoretical study was not able to completely reproduce the smooth, experimental voltage−capacity profile, particularly the presence of visible small voltage plateaus and a region near $x = 0.72$ in T#2−Li$_x$CoO$_2$ where the potential changes rapidly with x. Therefore, the nature of superstructures present and lithium and vacancy ordering in T#2−Li$_x$CoO$_2$ are not fully understood and further experimental and theoretical studies are needed to confirm and elucidate the hypothesis.

Acknowledgment. National Science Foundation International Research Fellow Award INT 0000-429 is acknowledged. The authors thank Région Aquitaine for financial support. Fruitful discussions with Professor Gerbrand Ceder at MIT, Professor Jeffery Dahn at Dalhousie University, and Mr. Frédéric Tournadre at ICMCB-CNRS are greatly appreciated. Electron diffraction patterns reported in this study were collected at the Center of Electron Microscopy at Université Bordeaux I.

CM021816X

(21) Carlier, D.; Van der Ven, A.; Delmas, C.; Ceder, G. *Chem. Mater.*, in press.